CHEMISTRY OF MATERIALS

Article

pubs.acs.org/cm

Search for Organic Thermoelectric Materials with High Mobility: The Case of 2,7-Dialkyl[1]benzothieno[3,2-b][1]benzothiophene Derivatives

Wen Shi,[†] Jianming Chen,[‡] Jinyang Xi,[†] Dong Wang,*[,†] and Zhigang Shuai*[,†,‡]

[†]MOE Key Laboratory of Organic OptoElectronics and Molecular Engineering, Department of Chemistry, Tsinghua University, Beijing 100084, People's Republic of China

[‡]Key Laboratory of Organic Solids, Beijing National Laboratory for Molecular Science (BNLMS), Institute of Chemistry, Chinese Academy of Sciences, Beijing 100190, People's Republic of China

Supporting Information

ABSTRACT: Control of doping is crucial for enhancing the thermoelectric efficiency of a material. However, doping of organic semiconductors often reduces their mobilities, making it challenging to improve the thermoelectric performance. Targeting on this problem, we propose a simple model to quantitatively obtain the optimal doping level and the peak value of thermoelectric figure of merit (zT) from the intrinsic carrier mobility, the lattice thermal conductivity, and the effective density of states. The model reveals that high intrinsic mobility and low lattice thermal conductivity give rise to a low optimal doping level and a high maximum zT. To demonstrate how the model works, we investigate, from first-principles calculations, the thermoelectric properties of a novel class of excellent hole transport organic materials, 2,7-dialkyl[1]benzothieno[3,2-b][1]benzothiophene derivatives (C_n-BTBTs). The first-principles calculations show that BTBTs exhibit high mobilities, extremely low thermal conductivities (~0.2 W m^{-1} K^{-1}), and large Seebeck coefficients (~0.3 mV K^{-1}), making them ideal candidates for thermoelectric applications. Moreover, the maximum zT predicted from the simple model agrees with that observed from the first-principles calculations. This study has provided new insights to guide the search for organic thermoelectric materials and their optimization.

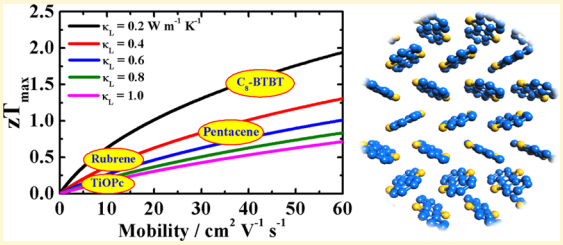

1. INTRODUCTION

The use of thermoelectric (TE) materials to harvest electricity from waste heat via the Seebeck effect has become increasingly important, because of the global need for energy production and conservation.[1−3] How big a role these TE energy converters are likely to play in solving the world's energy problems relies on how efficient these materials are. The energy conversion efficiency of a TE device is usually determined by an intrinsic material parameter known as the dimensionless TE figure of merit, zT:

$$zT = \frac{S^2\sigma T}{\kappa}$$

where S is the Seebeck coefficient, σ the electrical conductivity, T the average temperature of the hot and cold junctions, and κ the thermal conductivity. Both electrons and phonons are heat carriers. Therefore, $\kappa = \kappa_e + \kappa_L$ has two contributions: one is due to the electrons (κ_e), and the other arises from the lattice vibrations (κ_L). By definition, we see that a large Seebeck coefficient, a high electrical conductivity, and a low thermal conductivity are needed to achieve a high zT.

Despite their poor electrical conductivities, organic electronic materials have the advantages of having low thermal conductivities and low cost, and being solution-processable, flexible, and lightweight. Our previous first-principles investigations on closely packed molecular crystals and one-dimensional conducting polymer chains have shown that,[4] ideally, the best TE performance of these systems is even comparable to the state-of-the-art commercial bulk TE materials, such as Bi_2Te_3 and Sb_2Te_3 alloys, which exhibit a zT value in the range of 0.8−1.1 at room temperature.[5] Yet, the experimental zT value reported for both conducting polymers and small-molecule organic thin films is far less than our theoretical prediction. The TE properties of a variety of conducting polymers, such as polyacetylene,[6] polypyrroles,[7] polyanilines,[8] P3HT,[9] polycarbazoles,[10,11] and poly(metal 1,1,2,2-ethenetetrathiolate)s[12] were measured, but very low figures of merit were observed: until recently, zT values several orders of magnitude higher were reported. For example, for poly(3,4-ethylenedioxythiophene) (PEDOT), a maximum zT value of 0.42 has been achieved by minimizing the total dopant volume,[13] and a zT value of 0.25 achieved by accurate control of the oxidation level.[14] A series of metal coordination polymers containing 1,1,2,2-ethenetetrathiolate linking bridge showed

Received: February 5, 2014
Revised: March 16, 2014
Published: March 25, 2014

excellent *n*-type TE properties with a zT value of 0.2 at 440 K.[12] The TE properties of polymer composites[15,16] and nanoparticle-functionalized carbon nanotubes[17] were also reported.

Compared to conducting polymers, small-molecule organic semiconductors are advantageous in that they have well-defined structures and controllable properties, and they are easy to purify.[18−20] The TE properties of pentacene,[21−24] rubrene,[25] and phthalocyanines[26] have been experimentally studied. The newly discovered 2,7-dialkyl[1]benzothieno[3,2-b][1]-benzothiophene derivatives (C_n-BTBTs) show excellent air stability and high solubility in common organic solvents at room temperature.[18,27] The most exciting feature about C_n-BTBTs is that they usually show decent field-effect transistor characteristics with excellent hole transport properties. So far, the highest hole mobility reported for C_8−BTBT single-crystal films is 31.3 $cm^2\ V^{-1}\ s^{-1}$ at room temperature,[28] and the mobilities of C_n-BTBTs exhibit an order of C_{12}-BTBT > C_{10}-BTBT > C_8-BTBT.[29] Very recently, a mobility of 43 $cm^2\ V^{-1}\ s^{-1}$ was observed in a blended film of C_8-BTBT and polystyrene (PS).[30] Moreover, Tsukagoshi and co-workers showed that single-crystal C_8-BTBT displays the band-like transport behavior in the range of temperature from 160 K to 300 K, by measuring the temperature dependence of single-crystal FET mobility.[31] Itabashi and co-workers also demonstrated in theory that the band rather than hopping transport mechanism dominates in the single-crystal C_8-BTBT, even at room temperature.[32] They found that the hopping mobility of C_8-BTBT in a bulk single crystalline structure was less than 1 $cm^2\ V\ s^{-1}$, which contradicts the experimental measurement. For closely packed molecular crystals with high mobility such as polyacenes and BTBTs, it is reasonable to apply the band model to investigate the charge-transport properties of these materials.[33] Because of their excellent hole transport properties, BTBTs have attracted our attention as potential *p*-type TE materials. In this work, we investigate, theoretically, the TE properties of BTBTs.

Which electronic structure provides the largest zT value for TE materials? Mahan and Sofo have addressed this question, and they suggested that materials in which the distribution of energy carriers is as narrow as possible, but with high mobility in the direction of the applied electric field, show the maximum TE efficiency.[34] This offers criteria for the design of new TE materials. However, improving the TE performance of a given material by doping optimization remains crucial, as manifested by enhanced TE efficiency of PEDOT by engineered doping.[13,14] In this work, we first propose a simple model to quantitatively elucidate how to obtain the optimal doping level and the peak value of zT from the intrinsic mobility and the lattice thermal conductivity of a material. It is revealed that a high intrinsic mobility and low lattice thermal conductivity will lead to a low optimal doping level and high peak value of zT. Then, we study, from first-principles calculations, the TE properties of a novel class of excellent hole transport organic materials, C_n-BTBTs, and take C_8-BTBT as an example to demonstrate how the model works. BTBTs indeed exhibit high mobilities, extremely low thermal conductivities, and large Seebeck coefficients, which make them attractive for the TE applications. The maximum zT value predicted from the simple model coincides with that from the first-principles calculations.

2. METHODS

To evaluate zT from first-principles calculations, we performed the following three steps of calculations. First, we calculated the electronic structure and electron−phonon interactions using the first-principles method. The electron−phonon couplings were modeled by the deformation potential (DP) theory.[35] Second, we applied the Boltzmann transport theory to obtain the electrical transport coefficients. Third, we extracted the lattice thermal conductivity from the nonequilibrium molecular dynamics (NEMD) simulations.[36,37]

2.1. Electronic Structure Calculations. Geometry optimization and the band structure calculations were performed by the projector augmented wave (PAW) method with the Perdew−Burke−Ernzerhof including dispersion (PBE-D) exchange correlation functional in the Vienna ab initio simulation package (VASP 5.3.2).[38−40] The cutoff energy for the plane-wave basis was set to be 600 eV. The convergence criterion of the total energy was set to be 10^{-5} eV in the self-consistent field iteration. The spin−orbit coupling was not considered. The Monkhorst−Pack **k**-mesh of 4 × 4 × 1 was used for the ionic and lattice constant relaxations and that of 8 × 8 × 2 was used for the single-point energy and charge density calculations. The tetrahedron method with Blöch corrections was used for smearing. The cutoff radius for pair interactions was set to be 50 Å throughout the calculations for C_8-BTBT, C_{10}-BTBT, and C_{12}-BTBT.

2.2. Boltzmann Transport Theory. We applied the Boltzmann transport equation (BTE) in the relaxation time approximation (RTA) to model the microscopic electrical transport process.[41,42] In the Boltzmann transport theory, the electrical transport coefficients—the electrical conductivity (σ), the Seebeck coefficient (S), and the electronic thermal conductivity (κ_e)—are all related to a transport distribution function,[4] $\sum_{\mathbf{k}} \mathbf{v}_{\mathbf{k}}\mathbf{v}_{\mathbf{k}}\tau_{\mathbf{k}}$, where $\tau_{\mathbf{k}}$ is the relaxation time, $\mathbf{v}_{\mathbf{k}} = \nabla_{\mathbf{k}}\varepsilon_{\mathbf{k}}/\hbar$ is the group velocity of an electron in a specified band, and $\varepsilon_{\mathbf{k}}$ is the band energy at a given **k**-point.

We can obtain the group velocity from the first-principles band structure calculations. To estimate the summation in the **k**-space, we followed Madsen and Singh's work and applied the smoothed Fourier interpolation method to obtain denser band energies.[43] The band energies on a fine **k**-mesh of 41 × 41 × 9 (amount to 3885 **k**-points in the irreducible Brillouin zone) were calculated for C_8-BTBT, C_{10}-BTBT, and C_{12}-BTBT. The original **k**-mesh was then interpolated onto a mesh 10 times denser. The electrical transport coefficients were calculated by the BoltzTraP[43,44] program, in which calculation of the relaxation times based on the DP theory was integrated.

2.3. DP Theory for Calculating the Relaxation Times. The relaxation times measure how quickly the electrons are restored to their equilibrium distribution via various scattering mechanisms. Here, we considered the longitudinal acoustic phonon scatterings in the long wavelength limit. Assuming that the scattering matrix element is independent of the direction of the lattice wave propagation, the relaxation time has the form

$$\frac{1}{\tau_{\mathbf{k}}} = \frac{2\pi}{\hbar}|M(\mathbf{k},\mathbf{k}')|^2 \sum_{\mathbf{k}'} \delta(\varepsilon_{\mathbf{k}} - \varepsilon_{\mathbf{k}'})(1 - \cos\theta) \quad (1)$$

where $\delta(\varepsilon_{\mathbf{k}} - \varepsilon_{\mathbf{k}'})$ is the Dirac delta function and θ the angle between **k** and **k**′. $|M(\mathbf{k},\mathbf{k}')|^2 = k_B T E_1^2/C_{ii}$ is the matrix element for electrons to be scattered from the Blöch state **k** to **k**′, where E_1 is the DP constant and C_{ii} is the elastic constant in the direction of the lattice wave propagation.[45−48] For the sake of simplicity, we stretched the unit cell along the crystal directions *a*, *b*, and *c*, respectively. E_1 was obtained by the linear fit of the band edge energy shift, with respect to the lattice dilation, and C_{ii} was obtained via the parabolic fit of the total energy with respect to the lattice dilation.

2.4. Molecular Dynamics Simulations of Phonon Transport. We applied the NEMD method to extract the lattice thermal conductivity. Our simulations were performed with the LAMMPS package.[49] In the NEMD simulations, a heat flux across the system was applied, and the resulting temperature gradient was measured after the system had established a steady state. The Müller−Plathe velocity-exchange algorithm was used to generate the heat flux in the system.[36,37] The GAFF was used to describe the bonded and nonbonded interactions of C_8-BTBT, C_{10}-BTBT, and C_{12}-BTBT. Periodic boundary conditions were applied in three dimensions. The

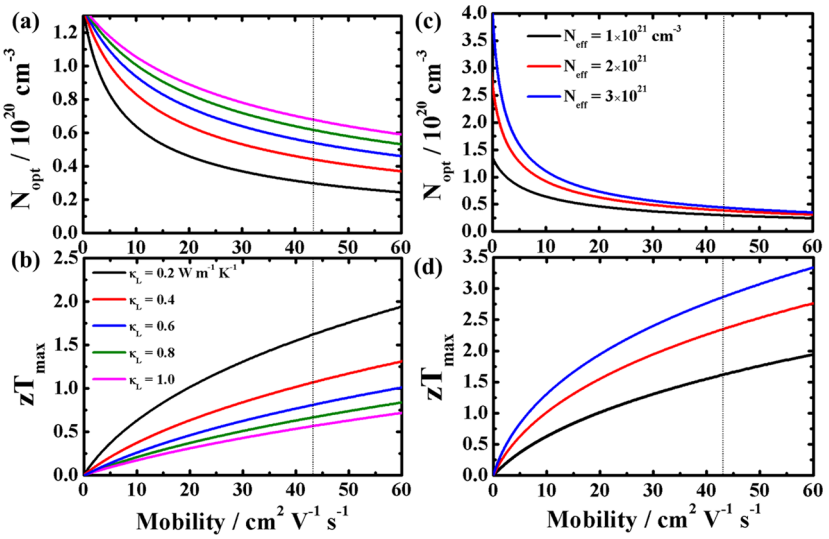

Figure 1. Dependence of (a) the optimal carrier concentration and (b) the corresponding maximum value of zT on the carrier mobility and the lattice thermal conductivity with the effective density of states fixed at N_{eff} = 10^{21} cm^{-3} under room temperature. Dependence of (c) the optimal carrier concentration and (d) the corresponding maximum value of zT on the carrier mobility and the effective density of states N_{eff} with the lattice thermal conductivity fixed at κ_L = 0.2 W m^{-1} K^{-1} under room temperature.

system was first equilibrated in the NPT ensemble for 500 ps with Nosé-Hoover thermostat and barostat at the temperature of 300 K and the pressure of 1 atm. The simulation box was divided into 20 layers along the direction of heat propagation. C_8-BTBT, C_{10}-BTBT, and C_{12}-BTBT are all monoclinic crystals and the division was done parallel to the box faces, so the heat propagates in the direction of a* and b*, respectively, instead of a and b. The total NEMD simulations lasted for 5 ns. The velocity swapping was performed every 1000 steps. The velocity Verlet algorithm was used to update the positions and velocities for atoms, and the time step was set to be 1 fs. To correct for the finite-size effect, we performed simulations at several box lengths, and then fit κ_{MD}^{-1} to L_{box}^{-1} to derive the lattice thermal conductivity of the true bulk crystal,[50,51] where κ_{MD} and L_{box} are the lattice thermal conductivity obtained from the NEMD simulations and the corresponding box length.

3. RESULTS AND DISCUSSION

Mahan and Sofo answered the question of what is the best electronic structure a TE material can have.[34] In this work, we raise a related question, which is how the intrinsic carrier mobility and lattice thermal conductivity affect the optimal doping level and peak value of zT of a given material? In the following, we propose a simple model to illustrate the dependencies of the optimal doping level and peak value of zT on the intrinsic carrier mobility and lattice thermal conductivity.

The general expression for the Seebeck coefficient neglecting the electron correlation effects can be written as[52]

$$S = -\frac{k_B}{e}\int \frac{E - E_F}{k_B T}\frac{\sigma(E)}{\sigma}\,dE \tag{2}$$

where k_B is the Boltzmann constant, e is the elementary charge, E_F is the Fermi level, T is the temperature, and σ is the electrical conductivity ($\sigma = \int \sigma(E)\,dE$). If the carrier only transports in the valence band, the Seebeck coefficient S is given by

$$S = \frac{k_B}{e}\left(\frac{E_F - E_v}{k_B T}\right) + A_v \tag{3}$$

where E_v is the valence band edge, A_v is a constant on the order of 1.[22,26,52] At low carrier concentrations with $E_F - E_v \gg k_B T$, A_v is negligibly small and the Boltzmann distribution is justified. The hole concentration (N_p) is then related to S by

$$N_p = N_{eff}\exp\left(-\frac{E_F - E_v}{k_B T}\right) = N_{eff}\exp\left[-\left(\frac{e}{k_B}\right)S\right]$$

where N_{eff} is the effective density of states.[26] After applying the relation $\sigma = N_p e\mu$ and the Wiedemann−Franz law ($\kappa_e = L\sigma T$ (we assume that the Lorentz number, 2.44 × 10^{-8} W Ω K^{-2}, is independent of the doping level)), we obtain the expression of zT as a function of carrier concentration:

$$zT = \frac{S^2\sigma T}{\kappa_e + \kappa_L} = \frac{k_B^2 \mu T}{e}\left[\frac{(\ln N_p - \ln N_{eff})^2 N_p}{L N_p e\mu T + \kappa_L}\right] \tag{4}$$

The condition $\partial zT/\partial N_p = 0$ yields the maximum dimensionless figure of merit

$$zT_{max} = \frac{4k_B^2 \mu T}{e}\frac{\left[LeT\left(\frac{\mu}{\kappa_L}\right)N_{opt} + 1\right]^2 N_{opt}}{L N_{opt} e\mu T + \kappa_L} \tag{5}$$

at the optimal carrier concentration

$$\ln N_{opt} = -2LeT\left(\frac{\mu}{\kappa_L}\right)N_{opt} + \ln N_{eff} - 2 \tag{6}$$

Assuming that the effective density of states is fixed, it can be observed from the above equation that a high intrinsic mobility and a low lattice thermal conductivity will lead to a low optimal carrier concentration. Quantitatively, we plot in Figure 1 the optimal doping level and the corresponding peak value of zT as a function of the intrinsic carrier mobility, the lattice thermal conductivity, and the effective density of states under room temperature. For organic materials, the lattice thermal conductivity κ_L usually falls in the range of 0.1−1.0 W m^{-1} K^{-1}. The magnitude of the effective density of states is usually on the order of 10^{21} cm^{-3}; according to the literature, compounds such as pentacene, vanadyl-phthalocyanine, and naphthalenetetracarboxylic dianhydride have values of 2.9 ×

dx.doi.org/10.1021/cm500429w | Chem. Mater. 2014, 26, 2669−2677

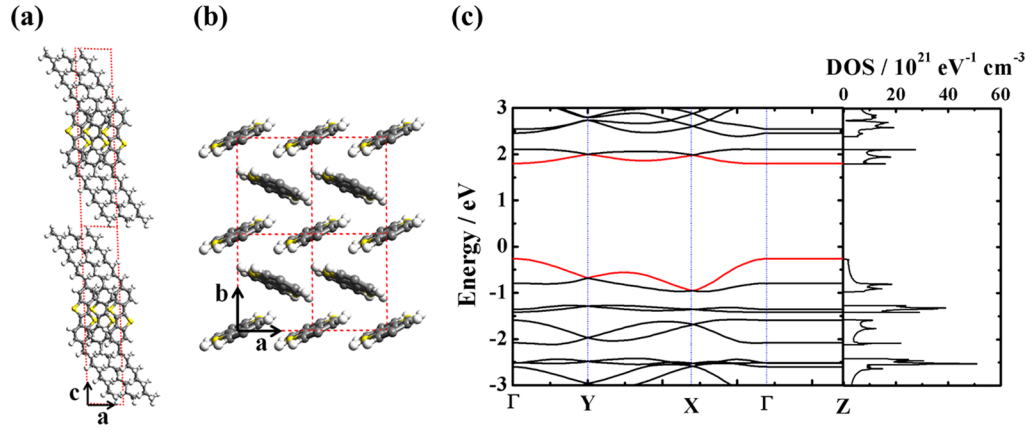

Figure 2. (a) Lamella-like alternating structure of C_8-BTBT in the *ac* plane. (b) Herringbone arrangement of C_8-BTBT in the *ab* plane; the red dashed lines represent the crystal lattices. (For the sake of clarity, the alkyl chains have been omitted in panel b. The lattice vectors *a* and *c* are nonorthogonal, but *a* and *b* are orthogonal.) (c) Band structures and DOS of C_8-BTBT; the band energies are shifted relative to the Fermi level. The reciprocal coordinates of high-symmetry points are Γ = (0, 0, 0), Y = (0, 0.5, 0), X = (0.5, 0, 0), and Z = (0, 0, 0.5). The highest valence band and lowest conduction band are highlighted in red.

10^{21} cm^{-3}, 1.6 × 10^{21} cm^{-3}, and 2.0 × 10^{21} cm^{-3}, respectively.[22,26,53] The black dotted vertical line in Figure 1 represents the highest mobility reported to date for organic materials: μ = 43 cm^2 V^{-1} s^{-1} for C_8-BTBT:PS blended films.[30] As shown in Figure 1b, if the carrier mobility increases to 10 cm^2 V^{-1} s^{-1}, the lattice thermal conductivity reduces to 0.2 W m^{-1} K^{-1} and the effective density of states is 10^{21} cm^{-3}, the peak value of zT will exceed 0.5 easily. The TE properties of 2,3,5,6-tetrafluoro-7,7,8,8-tetracyanoquinodimethane (F_4-TCNQ) and iodine-doped pentacene thin films and F_4-TCNQ-doped pentacene in a bilayer structure have been studied experimentally. Although the carrier concentration in doped pentacene is high (10^{20}–10^{21} cm^{-3}), the TE efficiency is very low, which can be ascribed to the extremely low mobility of the doped pentacene, usually falling in the range of 0.01–1 cm^2 V^{-1} s^{-1} under room temperature.[21,23,24] It is known that pentacene has high intrinsic mobility, but for TE applications, it must be doped for enhanced TE efficiency. The dilemma is that the dopants, such as F_4-TCNQ and iodine, not only increase the carrier concentration, but also substantially decrease the mobility of conducting host molecules, because they often increase the distance between neighboring host molecules and thereby reduce the electronic coupling.

The above model analysis at low carrier concentrations shows that the high intrinsic mobility of the material gives rise to a low optimal doping level and a high peak value of zT. Because of the difficulty and inefficiency for doping of organic semiconductors, we propose to search for organic thermoelectric materials with high mobility. If the mobility is high, the optimal doping level will be low, which indicates that less volume of dopants is needed and there is less of an effect of dopants on the charge-transport properties of organic semiconductors. In addition to the mobility and lattice thermal conductivity, the large effective density of states leads to the high maximum zT value, which is consistent with Mahan and Sofo's point of view;[34] unfortunately, it leads to the high optimal doping level at the same time. In the following, we study, from first-principles calculations, the TE performance of a novel class of *p*-type organic semiconductors with high mobility—C_8-BTBT, C_{10}-BTBT, and C_{12}-BTBT—and take C_8-BTBT as an example to demonstrate how the simple model works.

The BTBT crystals exhibit a lamella-like structure with the alkyl layers and the BTBT layers aligning alternatively along the *c*-direction (see Figure 2a). In the *ab* plane, the BTBT cores form a herringbone arrangement, which facilitates the two-dimensional (2D) charge transport (see Figure 2b). The optimized lattice constants have been collected in Table S1 in the Supporting Information; they are shorter than the experimental ones, and the deviations are largely within 5%.[29] Actually, the geometry optimization has also been performed with the local density approximation (LDA) exchange correlation functional, but the results are poorer than those obtained with the PBE-D exchange correlation functional. It shows that inclusion of the dispersion correction in the study of organic materials is necessary, in which the van der Waals interactions dominate.[54] As observed in the crystal structures, the optimized lattice constants *a* and *b* decrease with increasing length of alkyl chains,[29] which means that the BTBT cores pack more closely along the *a*- and *b*-axes with longer alkyl chains. This has been explained by Takimiya and co-workers as stronger hydrophobic interactions between longer alkyl chains.[29]

C_8-BTBT, C_{10}-BTBT, and C_{12}-BTBT are all direct-band-gap semiconductors with the band-gap opening at the Γ-point. (See Figure 2c and Figure S1 in the Supporting Information.) The calculated band gaps of these three crystals are 2.060 eV, 2.000 eV, and 2.003 eV, respectively. The highest valence band (VB) of C_8-BTBT, C_{10}-BTBT, and C_{12}–BTBT exhibits the largest bandwidth along the ΓX direction, which is 0.689 eV, 0.722 eV, and 0.720 eV (see Table S2 in the Supporting Information for the bandwidths along other high-symmetry directions). The bandwidth of the highest VB in BTBTs is significantly larger than that of the lowest conduction band (CB), which suggests that the hole transport dominates in these materials, in accordance with the experimental observations. For the lightly doped organic semiconductors studied in this work, only the highest VB and lowest CB contribute to the charge transport. The wide band feature of the highest VB suggests that the electronic states are delocalized, and the band instead of hopping transport mechanism dominates. The bandwidths of both VB and CB along the ΓZ direction are exactly zero, which also confirms the 2D transport behavior in these crystals. In addition, the bandwidths of both CB and VB become larger

dx.doi.org/10.1021/cm500429w | *Chem. Mater.* 2014, 26, 2669–2677

when going from C_8-BTBT to C_{10}-BTBT, but the change is not obvious when going from C_{10}-BTBT to C_{12}-BTBT.

To calculate the elastic constant C_{ii}, we stretched the unit cell of C_8-BTBT, C_{10}-BTBT, and C_{12}-BTBT along the *a*-, *b*-, and *c*-directions, respectively, by ±0.5%, ± 1.0%, ± 1.5%, and ±2.0%, and calculate the total energy change due to the unit-cell deformation. The elastic constant C_{ii} can be obtained by fitting the total energy E with respect to the dilation $\Delta l/l_0$, using the formula

$$\frac{E - E_0}{V_0} = C_{ii}\frac{(\Delta l/l_0)^2}{2}$$

Here, V_0 and E_0 are, respectively, the volume and total energy of the unit cell at equilibrium. Δl is the change of lattice constant along the direction *ii* (i = *a*, *b*, *c*), and l_0 is its value at equilibrium. To obtain the DP constant E_1 in each lattice direction, we calculate the band energies with the lattice deformed in that direction, and fit the band-edge positions of VB and CB to the dilation $\Delta l/l_0$ with the formula $E_1 = \Delta E_{CB(VB)}/(\Delta l/l_0)$. Here, $\Delta E_{CB(VB)}$ is the change in band-edge position, relative to the lattice dilation $\Delta l/l_0$. Since in calculating the band energy in the bulk crystal by VASP, the reference zero-point of the energy is unknown, it is difficult to obtain the absolute energy change from two calculations with different lattice constants. Therefore, we adopt an approximation proposed by Wei and Zunger,[55] who assumed that the lowest energy band was barely influenced by the slight lattice deformation and it can be taken as an energy reference to calculate the band energy shift of the VB and CB. The calculated DP constant E_1 for electrons and holes, and the elastic constant C_{ii} for C_8-BTBT, C_{10}-BTBT, and C_{12}-BTBT along the *a*-, *b*-, and *c*-directions are listed in Table 1. It is observed that, for these three compounds, both DP constant and elastic constant are apparently anisotropic.

Table 1. DP Constants (E_1) and Elastic Constants (C_{ii}) for Electrons and Holes in C_8-BTBT, C_{10}-BTBT, and C_{12}-BTBT along the *a*-, *b*-, and *c*-Directions

direction	DP constant, E_1 (eV)	elastic constant, C_{ii} ($\times 10^9$ J m^{-3})
	C_8-BTBT	
a	2.29 (e) 1.39 (h)	18.3
b	0.74 (e) 2.73 (h)	9.76
c	0.78 (e) 0.47 (h)	37.4
	C_{10}-BTBT	
a	2.44 (e) 1.41 (h)	15.1
b	0.88 (e) 2.82 (h)	10.2
c	1.05 (e) 0.61 (h)	45.0
	C_{12}-BTBT	
a	2.52 (e) 1.43 (h)	19.4
b	0.83 (e) 2.92 (h)	10.1
c	0.74 (e) 1.16 (h)	61.6

Based on the band structures from first-principles calculations, we calculated the electrical transport coefficients by solving the BTE within the RTA. We adopted two schemes to derive the relaxation times. One is based on the DP theory, and the alternative is to take the relaxation time as an empirical parameter, which can be derived by comparison between the theoretical and experimental mobilities.[56] For the first scheme, the scattering matrix elements averaged over three lattice directions (*a*, *b*, and *c*) are used to calculate the relaxation times. The calculated average relaxation times τ of electrons and holes for C_8-BTBT, C_{10}-BTBT, and C_{12}-BTBT at 298 K are summarized in Table S3 in the Supporting Information. As that table shows, for each of three compounds, the relaxation times of holes are significantly larger than those of electrons, which indicates that the mobility of holes is larger and also proves that BTBTs are typical hole transport materials. It is found that as the alkyl chains are elongated, both the electron and hole relaxation times increase. For the second scheme, the hole relaxation time τ averaged over crystal directions *a* and *b* is 19.9 fs, which is derived by fitting the experimental mobility μ = 31.3 cm^2 V^{-1} s^{-1} of single-crystal C_8-BTBT at room temperature[28] to our theoretical mobilities derived from the relation $\sigma = N_p e\mu$. The relaxation times for holes based on the DP theory are on the order of 100 fs, which are 5−6 times larger than that empirically derived.

The Seebeck coefficient (S), the electrical conductivity (σ), the electronic thermal conductivity (κ_e), and the TE power factor ($S^2\sigma$) in the *ab* plane for C_8-BTBT, C_{10}-BTBT, and C_{12}-BTBT at 298 K are shown in Figure 3 and Figure S2 in the Supporting Information, as a function of the carrier concentration, with the relaxation times derived in a first-principles manner from the DP theory. It is noted that the electrical transport coefficients are almost isotropic for both electrons and holes, and the maximum power factors $S^2\sigma$ for holes are larger than those for electrons, because of the much

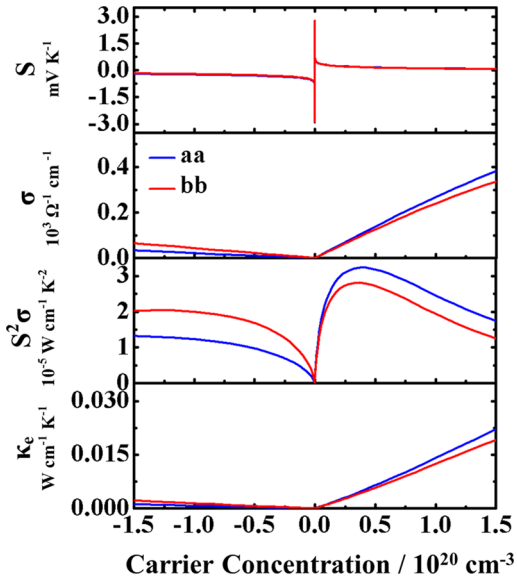

Figure 3. Seebeck coefficient (S), electrical conductivity (σ), TE power factor ($S^2\sigma$), and electronic thermal conductivity (κ_e) along the *a*-direction (blue lines) and the *b*-direction (red lines) for C_8-BTBT, as a function of carrier concentration at 298 K. The relaxation times were calculated from the DP theory. The carrier concentration is positive for *p*-type doping and negative for *n*-type doping.

dx.doi.org/10.1021/cm500429w | *Chem. Mater.* 2014, 26, 2669−2677

higher electrical conductivities σ for holes than for electrons. This indicates that C_8-BTBT, C_{10}-BTBT, and C_{12}-BTBT are all *p*-type TE materials. As the length of alkyl chains increases, the maximum power factors $S^2\sigma$ remain almost unchanged, as do the largest Seebeck coefficients *S*.

The slope of the $\sigma-N$ curve in the linear region gives the carrier mobility, according to the relation $\sigma = Ne\mu$. From Figure 3 and Figure S2 in the Supporting Information, we extracted the electron and hole mobilities μ for C_8-BTBT, C_{10}-BTBT, and C_{12}-BTBT (see Table 2). It is seen that the hole mobility is

Table 2. Calculated Electron and Hole Mobility (μ) for C_8-BTBT, C_{10}-BTBT, and C_{12}-BTBT along the *a*- and *b*-Directions at 298 K

	C_8-BTBT	C_{10}-BTBT	C_{12}-BTBT
Hole Mobility ($cm^2\ V^{-1}\ s^{-1}$)			
μ_a^h	180	194	211
μ_b^h	165	174	199
Electron Mobility ($cm^2\ V^{-1}\ s^{-1}$)			
μ_a^e	13.4	12.2	16.4
μ_b^e	28.1	25.4	34.7

indeed significantly larger than the electron mobility along both the *a*- and *b*-directions, indicating that BTBTs are hole transport materials. The mobility of holes is almost isotropic for all three compounds, which is consistent with previous theoretical predictions,[57] and recent experimental observations for C_8-BTBT:PS film.[30] Furthermore, as the length of alkyl chains increases, the hole mobility increases, which agrees qualitatively well with the experimental observation.[29] The mobilities calculated for holes are 5−6 times higher than the experimental value; a value of 31.3 $cm^2\ V^{-1}\ s^{-1}$ was reported for single-crystal C_8-BTBT at room temperature.[28] Such a discrepancy can be attributed to the fact that (i) only the longitudinal acoustic phonon scatterings are taken into account in the calculation of relaxation times and (ii) the optimized lattice constants are smaller than those observed in the crystal structures. The relaxation times derived from the DP theory, and the mobilities subsequently calculated are apparently overestimated, because of the neglect of optical phonon scatterings.

To fully characterize a TE material, it is essential to obtain its lattice thermal conductivity (κ_L). We extracted the κ_L value of C_8-BTBT, C_{10}-BTBT, and C_{12}-BTBT along the *a**- and *b**-directions from the NEMD simulations. We build the supercells with different lengths in the direction of *a** and *b**. Each supercell is divided into 20 layers, labeled as layers 0, 1, ..., 19 from left to right. The local temperature of layers 0−10 and the instantaneous temperature for layer 0 (the heat sink) and layer 10 (the heat source) are plotted in Figure 4 and its inset. It is found that, as the simulation proceeds, the temperature of layer 0 drops, and that of layer 10 rises. After 1 ns, the steady state and the local thermal equilibrium have been reached. The local temperature of each layer is obtained by taking an average over trajectories from 1 ns to 5 ns. As shown in Figure 4, the linear relationship between the temperature and the layer number is very good except for the region near the heat sink (layers 0 and 1) and the heat source (layers 9 and 10), because the unphysical exchange of atomic velocities and the physical heat flow in the system are not well-balanced. The temperature gradient is then obtained by fitting the curve in the linear region. To correct the size effect, we perform the NEMD

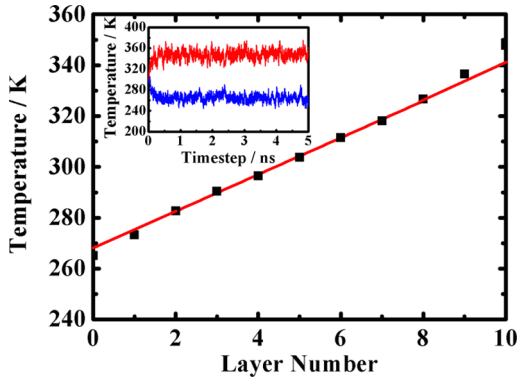

Figure 4. Temperature profile of C_8-BTBT along the *a**-direction obtained from the NEMD simulations for box dimensions of 20 × 3 × 1. The time average has been taken over the final 4 ns of the simulation. The solid red line represents a linear fit of the data. The inset shows the temperature evolution with time for the heat sink (blue) and heat source (red).

simulations with different box lengths in the direction of *a** and *b** (see Figure S3 in the Supporting Information). We extract the lattice thermal conductivity of the true bulk crystal by fitting κ_{MD}^{-1} to L_{box}^{-1} and extrapolating. Table 3 lists the lattice

Table 3. Calculated Lattice Thermal Conductivity (κ_L) for C_8-BTBT, C_{10}-BTBT, and C_{12}-BTBT along the *a- and *b**-Directions at 300 K**

	κ_L ($W\ m^{-1}\ K^{-1}$)	
	*a**-direction	*b**-direction
C_8-BTBT	0.18	0.18
C_{10}-BTBT	0.18	0.18
C_{12}-BTBT	0.25	0.22

thermal conductivities (κ_L) for C_8-BTBT, C_{10}-BTBT, and C_{12}-BTBT at 300 K, with the magnitude falling in the range of 0.18−0.25 $W\ m^{-1}\ K^{-1}$. Compared to inorganic TE materials, the lattice thermal conductivity of BTBTs is extraordinarily small, although the all-scale hierarchical architecture method has been used to reduce the lattice thermal conductivity of PbTe to ∼0.6 $W\ m^{-1}\ K^{-1}$.[58] So far, there is no experimental result available for the thermal conductivity of crystalline C_n-BTBTs. The thermal conductivity of pentacene, *N*,*N*′-diphenyl-*N*,*N*′-di(3-methylphenyl)-(1,1′-biphenyl)-4,4′-diamine (TPD), and tris(8-hydroquinolinato)aluminum (Alq_3) thin films were measured to be 0.51 $W\ m^{-1}\ K^{-1}$, 0.24 $W\ m^{-1}\ K^{-1}$, and 0.48 $W\ m^{-1}\ K^{-1}$, respectively.[59] Compared with these small-molecule organic materials, the thermal conductivities of BTBTs are also smaller. This is because the alkyl side chains of BTBTs give rise to more low-frequency phonon modes, which contribute more to the phonon−phonon scatterings and lead to the reduced lattice thermal conductivity.[60,61] Our previous theoretical study on the anisotropic thermal transport in the pentacene crystal shows that the lattice thermal conductivity of pentacene is 0.72 $W\ m^{-1}\ K^{-1}$, 1.1 $W\ m^{-1}\ K^{-1}$, and 0.61 $W\ m^{-1}\ K^{-1}$, respectively, along the three reciprocal lattice directions.[61] In addition, the lattice thermal conductivity of phthalocyanine (H_2PC) along the closest packing direction is calculated to be 2.1 $W\ m^{-1}\ K^{-1}$ in our previous work.[62] The lattice thermal conductivities of C_n-BTBTs are 4−5 times lower than that of pentacene along the dominant transport direction, which is due to the introduction of long alkyl side chains in BTBTs as explained above. Table 3

dx.doi.org/10.1021/cm500429w | *Chem. Mater.* 2014, 26, 2669−2677

also shows little in-plane anisotropy of phonon transport for C_n-BTBTs. The extremely low lattice thermal conductivity apparently favors TE transport in these materials. According to the model that we proposed earlier, we speculate that C_n-BTBTs require a low doping level to achieve the optimal TE efficiency, because of its ultralow lattice thermal conductivity but ultrahigh hole mobility.

Combining the lattice thermal conductivity with the electrical transport coefficients, we finally obtained the dimensionless figure of merit (zT) as a function of the carrier concentration for C_8-BTBT, C_{10}-BTBT, and C_{12}-BTBT along the *a*- and *b*-directions (see Figure 5). When *p*-doped, the peak zT values

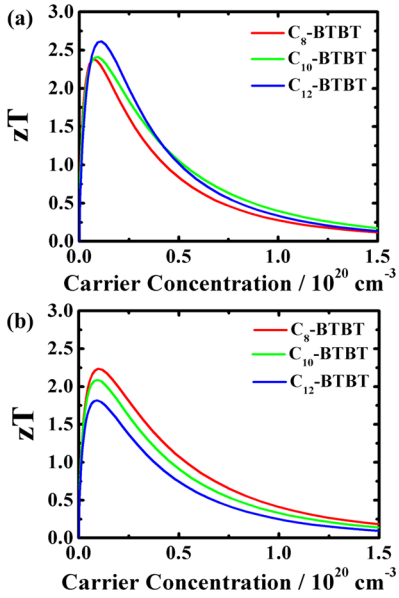

Figure 5. Calculated dimensionless thermoelectric figure of merit (zT) versus the hole concentration for C_8-BTBT, C_{10}-BTBT, and C_{12}-BTBT along the (a) *a*-direction and (b) *b*-direction under room temperature.

for C_8-BTBT, C_{10}-BTBT, and C_{12}-BTBT are 2.4, 2.4, and 2.6 along the *a*-direction at doping levels of 9.8×10^{18} cm^{-3}, 9.3×10^{18} cm^{-3}, and 11×10^{18} cm^{-3}, respectively. In the *b*-direction, the peak zT values are 2.2, 2.1, and 1.8 at doping levels of 9.8×10^{18} cm^{-3}, 9.3×10^{18} cm^{-3}, and 9.3×10^{18} cm^{-3}, respectively (see Table 4 and Table S4 in the Supporting Information). The zT value obtained based on the relaxation times derived from the DP theory, which are overestimated due to the neglection of optical phonon scatterings, gives the upper boundary of our theoretical prediction. When an empirical relaxation time of 19.9 fs was supplied for C_8-BTBT, the peak zT value was 0.73 at the optimal doping level of 22×10^{18} cm^{-3} (see Figure 6 and Table 4), which gives the lower boundary of our theoretical prediction. At the optimal doping level, the Seebeck coefficients

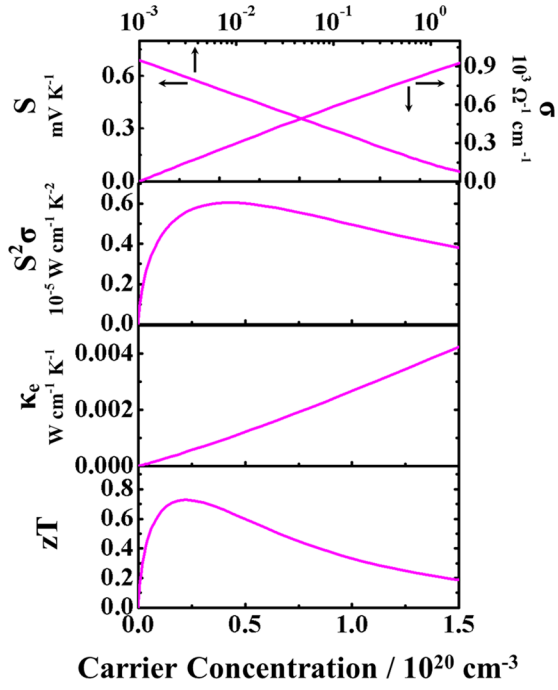

Figure 6. Electrical transport coefficients averaged over the *a*- and *b*-directions and the zT value for C_8-BTBT as a function of the hole concentration at 298 K. These TE transport coefficients were obtained based on an empirical relaxation time τ = 19.9 fs, which was derived by fitting the experimental mobility μ (31.3 cm^2 V^{-1} s^{-1}) of single-crystal C_8-BTBT to our calculated value. The Seebeck coefficient (S) was plotted versus the logarithm of the hole concentration.

of these materials are all ~300 μV K^{-1}, which coincide with those reported for small-molecule organic semiconductors, such as F_4-TCNQ doped pentacene at room temperature.[21] The large Seebeck coefficients are due to the sharp DOS feature of the VB and CB. By comparing the results for C_8-BTBT based on two schemes to derive the relaxation times, we noted that, with the lattice thermal conductivity and the effective density of states fixed, when the mobility is low, the peak zT value is low, while the optimal doping level is high (see Table 4). This is in accordance with the conclusion drawn from the model that we proposed: the TE material with high mobility possesses a high peak zT value and a low optimal doping level. It should be noted that since the electrical transport coefficients calculated are all intrinsic properties of the pristine materials without explicitly taking into account the influence of dopants, the absolute value of zT reported here is usually overestimated. When the intrinsic mobility, the lattice thermal conductivity, and the effective density of states of C_8-BTBT are supplied as parameters to the simple model, we can predict the optimal doping level and maximum zT value, and the values agree

Table 4. Optimal Doping Level and Peak zT Value for C_8−BTBT at Room Temperature[a]

	direction	S (mV K^{-1})	σ (Ω^{-1} cm^{-1})	$S^2\sigma$ (μW cm^{-1} K^{-2})	κ_e(W m^{-1} K^{-1})	peak zT value	optimal doping level ($\times 10^{18}$ cm^{-3})
DP model	*a*	0.29	280	23.5	0.12	2.4	9.8
	b	0.29	257	21.0	0.10	2.2	9.8
empirical	average	0.22	110	5.57	0.05	0.73	22

[a]The electrical transport coefficients at the optimal doping level were provided. The relaxation time was either derived from the DP theory or supplied as an empirical parameter.

dx.doi.org/10.1021/cm500429w | *Chem. Mater.* 2014, 26, 2669−2677

reasonably well with those from the first-principles calculations, which validates the model proposed.

4. CONCLUSIONS

The enhanced TE efficiency of PEDOT by accurate control of the oxidation level and the dopant volume[13,14] suggests that organic semiconductors can be potentially good TE materials. However, doping optimization for improved TE properties is still challenging practically, and a deep understanding of the various factors that govern the TE properties of organics materials is important.

In this work, by constructing a simple model, we quantitatively obtain the optimal doping level and the peak zT value from the intrinsic mobility, the effective density of states, and the lattice thermal conductivity. The intrinsic mobility and the effective density of states are related to the electronic structure of a material, and the lattice thermal conductivity is related to the lattice vibration. All of these are intrinsic properties of pristine materials. The model shows that a high intrinsic mobility and low lattice thermal conductivity will lead to a low optimal doping level and high peak zT value. The finding gives us important hints in the search for new organic thermoelectric materials and their optimization. From the theoretical perspective, the high intrinsic mobility calls for the strong intermolecular electronic coupling, which often calls for the short molecular stacking distance. The molecular packing in organic semiconductors can be tuned by introducing long alkyl side chains, as shown in the case of C_n-BTBTs, and by using lattice strains as demonstrated in TIPS-pentacene.[63] Moreover, reducing the grain boundaries, impurities, and defects in organic materials will also help to enhance the mobility.

For organic semiconductors that are loosely bonded by van der Waals interactions, doping is necessary to obtain sufficient charge carrier density, but at the same time, it often decreases their mobilities. Considering the dilemma of the doping control and the mobility of conducting molecules, we propose to search for organic thermoelectric materials with high intrinsic mobility and low lattice thermal conductivity, which tend to have a low optimal doping level and a high figure of merit. If a small amount of dopants are needed, the negative effect of doping on the charge transport properties can be minimized.

As a demonstration of how the model works, we investigate, from first-principles calculations, the TE properties of C_n-BTBTs with varying alkyl chain lengths. C_8-BTBT has been reported to have the highest mobility in all organic materials. We find that C_n-BTBTs not only exhibit high mobilities, but also large Seebeck coefficients and extremely low lattice thermal conductivities (0.18−0.25 W m^{-1} K^{-1}), because of the introduction of long alkyl chains. The lattice thermal conductivities of BTBTs have reached the practical lower limit for semiconductors: 0.2 W m^{-1} K^{-1}.[64] When estimated using the single-crystal mobility of C_8-BTBT (31.3 cm^2 V^{-1} s^{-1}), the peak zT value reaches 0.73 at an optimal doping level of 22×10^{18} cm^{-3}. These values are consistent with those predicted from the simple model, using the properties of undoped BTBTs. Our study suggests that if controlled doping is achieved without significantly decrease of the charge transport properties of the materials, BTBTs will become a novel class of organic materials, showing remarkable potentials for the TE applications.

■ ASSOCIATED CONTENT

Supporting Information

Optimized and experimental lattice constants, band dispersions, and relaxation times of BTBTs. This material is available free of charge via the Internet at http://pubs.acs.org.

■ AUTHOR INFORMATION

Corresponding Authors

*E-mail: dong913@tsinghua.edu.cn (D.W.).
*E-mail: zgshuai@tsinghua.edu.cn (Z.S.).

Notes

The authors declare no competing financial interest.

■ ACKNOWLEDGMENTS

This work is supported by the National Natural Science Foundation of China (Grant Nos. 21273124 and 21290190) and the Ministry of Science and Technology of China (Grant No. 2013CB933503). Computational resources were provided by the Tsinghua Supercomputing Center.

■ REFERENCES

(1) DiSalvo, F. J. *Science* **1999**, *285*, 703.
(2) Bell, L. E. *Science* **2008**, *321*, 1457.
(3) Gaultois, M. W.; Sparks, T. D.; Borg, C. K. H.; Seshadri, R.; Bonificio, W. D.; Clarke, D. R. *Chem. Mater.* **2013**, *25*, 2911.
(4) Wang, D.; Shi, W.; Chen, J.; Xi, J.; Shuai, Z. *Phys. Chem. Chem. Phys.* **2012**, *14*, 16505.
(5) Snyder, G. J.; Toberer, E. S. *Nat. Mater.* **2008**, *7*, 105.
(6) Pukacki, W.; Płocharski, J.; Roth, S. *Synth. Met.* **1994**, *62*, 253.
(7) Kemp, N. T.; Kaiser, A. B.; Liu, C. J.; Chapman, B.; Mercier, O.; Carr, A. M.; Trodahl, H. J.; Buckley, R. G.; Partridge, A. C.; Lee, J. Y.; Kim, C. Y.; Bartl, A.; Dunsch, L.; Smith, W. T.; Shapiro, J. S. *J. Polym. Sci., Part B: Polym. Phys.* **1999**, *37*, 953.
(8) Sun, Y.; Wei, Z.; Xu, W.; Zhu, D. *Synth. Met.* **2010**, *160*, 2371.
(9) Xuan, Y.; Liu, X.; Desbief, S.; Leclère, P.; Fahlman, M.; Lazzaroni, R.; Berggren, M.; Cornil, J.; Emin, D.; Crispin, X. *Phys. Rev. B* **2010**, *82*, 115454.
(10) Lévesque, I.; Bertrand, P.-O.; Blouin, N.; Leclerc, M.; Zecchin, S.; Zotti, G.; Ratcliffe, C. I.; Klug, D. D.; Gao, X.; Gao, F.; Tse, J. S. *Chem. Mater.* **2007**, *19*, 2128.
(11) Aïch, R. B.; Blouin, N.; Bouchard, A.; Leclerc, M. *Chem. Mater.* **2009**, *21*, 751.
(12) Sun, Y.; Sheng, P.; Di, C.; Jiao, F.; Xu, W.; Qiu, D.; Zhu, D. *Adv. Mater.* **2012**, *24*, 932.
(13) Kim, G. H.; Shao, L.; Zhang, K.; Pipe, K. P. *Nat. Mater.* **2013**, *12*, 719.
(14) Bubnova, O.; Khan, Z. U.; Malti, A.; Braun, S.; Fahlman, M.; Berggren, M.; Crispin, X. *Nat. Mater.* **2011**, *10*, 429.
(15) Zhang, K.; Zhang, Y.; Wang, S. *Sci. Rep.* **2013**, *3*, 3448.
(16) Zhang, K.; Davis, M.; Qiu, J.; Hope-Weeks, L.; Wang, S. *Nanotechnology* **2012**, *23*, 385701.
(17) Zhang, K.; Wang, S. *Carbon* **2014**, *69*, 46.
(18) Ebata, H.; Izawa, T.; Miyazaki, E.; Takimiya, K.; Ikeda, M.; Kuwabara, H.; Yui, T. *J. Am. Chem. Soc.* **2007**, *129*, 15732.
(19) Herwig, P. T.; Müllen, K. *Adv. Mater.* **1999**, *11*, 480.
(20) Jo, P. S.; Vailionis, A.; Park, Y. M.; Salleo, A. *Adv. Mater.* **2012**, *24*, 3269.
(21) Harada, K.; Sumino, M.; Adachi, C.; Tanaka, S.; Miyazaki, K. *Appl. Phys. Lett.* **2010**, *96*, 253304.
(22) Kim, G. H.; Shtein, M.; Pipe, K. P. *Appl. Phys. Lett.* **2011**, *98*, 093303.
(23) Hayashi, K.; Shinano, T.; Miyazaki, Y.; Kajitani, T. *Phys. Status Solidi C* **2011**, *8*, 592.
(24) Hayashi, K.; Shinano, T.; Miyazaki, Y.; Kajitani, T. *J. Appl. Phys.* **2011**, *109*, 023712.

(25) Pernstich, K. P.; Rossner, B.; Batlogg, B. *Nat. Mater.* **2008**, *7*, 321.
(26) Pfeiffer, M.; Beyer, A.; Fritz, T.; Leo, K. *Appl. Phys. Lett.* **1998**, *73*, 3202.
(27) Takimiya, K.; Shinamura, S.; Osaka, I.; Miyazaki, E. *Adv. Mater.* **2011**, *23*, 4347.
(28) Minemawari, H.; Yamada, T.; Matsui, H.; Tsutsumi, J.; Haas, S.; Chiba, R.; Kumai, R.; Hasegawa, T. *Nature* **2011**, *475*, 364.
(29) Izawa, T.; Miyazaki, E.; Takimiya, K. *Adv. Mater.* **2008**, *20*, 3388.
(30) Yuan, Y.; Giri, G.; Ayzner, A. L.; Zoombelt, A. P.; Mannsfeld, S. C. B.; Chen, J.; Nordlund, D.; Toney, M. F.; Huang, J.; Bao, Z. *Nat. Commun.* **2014**, *5*, 3005.
(31) Liu, C.; Minari, T.; Lu, X.; Kumatani, A.; Takimiya, K.; Tsukagoshi, K. *Adv. Mater.* **2011**, *23*, 523.
(32) Kobayashi, H.; Kobayashi, N.; Hosoi, S.; Koshitani, N.; Murakami, D.; Shirasawa, R.; Kudo, Y.; Hobara, D.; Tokita, Y.; Itabashi, M. *J. Chem. Phys.* **2013**, *139*, 014707.
(33) Shuai, Z.; Wang, L.; Li, Q. *Adv. Mater.* **2011**, *23*, 1145.
(34) Mahan, G. D.; Sofo, J. O. *Proc. Natl. Acad. Sci.* **1996**, *93*, 7436.
(35) Bardeen, J.; Shockley, W. *Phys. Rev.* **1950**, *80*, 72.
(36) Müller-Plathe, F. *J. Chem. Phys.* **1997**, *106*, 6082.
(37) Müller-Plathe, F.; Reith, D. *Comput. Theor. Polym. Sci.* **1999**, *9*, 203.
(38) Blöchl, P. E. *Phys. Rev. B* **1994**, *50*, 17953.
(39) Grimme, S. *J. Comput. Chem.* **2006**, *27*, 1787.
(40) Kresse, G.; Furthmüller, J. *Phys. Rev. B* **1996**, *54*, 11169.
(41) Scheidemantel, T. J.; Ambrosch-Draxl, C.; Thonhauser, T.; Badding, J. V.; Sofo, J. O. *Phys. Rev. B* **2003**, *68*, 125210.
(42) Yang, J.; Li, H.; Wu, T.; Zhang, W.; Chen, L.; Yang, J. *Adv. Funct. Mater.* **2008**, *18*, 2880.
(43) Madsen, G. K. H.; Singh, D. J. *Comput. Phys. Commun.* **2006**, *175*, 67.
(44) Madsen, G. K. H. *J. Am. Chem. Soc.* **2006**, *128*, 12140.
(45) Long, M.; Tang, L.; Wang, D.; Li, Y.; Shuai, Z. *ACS Nano* **2011**, *5*, 2593.
(46) Long, M.; Tang, L.; Wang, D.; Wang, L.; Shuai, Z. *J. Am. Chem. Soc.* **2009**, *131*, 17728.
(47) Chen, J.; Xi, J.; Wang, D.; Shuai, Z. *J. Phys. Chem. Lett.* **2013**, *4*, 1443.
(48) Tang, L.; Long, M.; Wang, D.; Shuai, Z. *Sci. China Ser. B: Chem.* **2009**, *52*, 1646.
(49) Plimpton, S. *J. Comput. Phys.* **1995**, *117*, 1.
(50) Schelling, P. K.; Phillpot, S. R.; Keblinski, P. *Phys. Rev. B* **2002**, *65*, 144306.
(51) Jiang, H.; Myshakin, E. M.; Jordan, K. D.; Warzinski, R. P. *J. Phys. Chem. B* **2008**, *112*, 10207.
(52) Fritzsche, H. *Solid State Commun.* **1971**, *9*, 1813.
(53) Nollau, A.; Pfeiffer, M.; Fritz, T.; Leo, K. *J. Appl. Phys.* **2000**, *87*, 4340.
(54) Bučko, T.; Hafner, J.; Lebègue, S.; Ángyán, J. G. *J. Phys. Chem. A* **2010**, *114*, 11814.
(55) Wei, S.; Zunger, A. *Phys. Rev. B* **1999**, *60*, 5404.
(56) Wang, D.; Tang, L.; Long, M.; Shuai, Z. *J. Chem. Phys.* **2009**, *131*, 224704.
(57) Northrup, J. E. *Appl. Phys. Lett.* **2011**, *99*, 062111.
(58) Biswas, K.; He, J.; Blum, I. D.; Wu, C.; Hogan, T. P.; Seidman, D. N.; Dravid, V. P.; Kanatzidis, M. G. *Nature* **2012**, *489*, 414.
(59) Kim, N.; Domercq, B.; Yoo, S.; Christensen, A.; Kippelen, B.; Graham, S. *Appl. Phys. Lett.* **2005**, *87*, 241908.
(60) Klemens, P. G. *Int. J. Thermophys.* **1981**, *2*, 55.
(61) Wang, D.; Tang, L.; Long, M.; Shuai, Z. *J. Phys. Chem. C* **2011**, *115*, 5940.
(62) Chen, J.; Wang, D.; Shuai, Z. *J. Chem. Theory Comput.* **2012**, *8*, 3338.
(63) Giri, G.; Verploegen, E.; Mannsfeld, S. C. B.; Atahan-Evrenk, S.; Kim, D. H.; Lee, S. Y.; Becerril, H. A.; Aspuru-Guzik, A.; Toney, M. F.; Bao, Z. *Nature* **2011**, *480*, 504.
(64) Spitzer, D. P. *J. Phys. Chem. Solids* **1970**, *31*, 19.